Hybrid GEO-PO Algorithm for Dual-Input Wireless Power Transfer and Photovoltaic-Fed DC-DC Converter in Electric Vehicle Charging Applications

Ganesh Babu M., *Student Member, IEEE*, and Srinivasa Rao Nayak P.

***Abstract*—The growing demand for efficient and sustainable electric vehicle (EV) charging solutions has accelerated the development of advanced multi-input power converter systems. This paper presents a closed-loop EV charger powered by dual energy sources wireless power transfer (WPT) and photovoltaic (PV) to enhance reliability and autonomy. The proposed non-isolated dual-input single-output (DISO) converter regulates output voltage using a proportional-integral (PI) controller to maintain constant voltage charging. To address the dynamic and nonlinear nature of the input sources, a novel Hybrid GEO-PO optimization algorithm is proposed, combining the exploration strength of the Golden Eagle Optimizer (GEO) and the exploitation ability of the Puma Optimizer (PO). The algorithm is used to optimally tune the PI controller gains, improving transient response and system stability. Simulation and experimental results in MATLAB/SIMULINK validate that the Hybrid GEO-PO outperforms both standalone GEO and PO algorithms in terms of overshoot reduction, faster settling time, and improved robustness. Compared to conventional methods like Ziegler-Nichols tuning, the proposed technique offers enhanced adaptability and dynamic performance. Furthermore, FPGA-based hardware implementation confirms real-time feasibility. This work positions the Hybrid GEO-PO algorithm as a promising optimization framework for future intelligent, self-reliant EV charging infrastructure integrating renewable sources.**

Link to graphical and video abstracts, and to code: https://latamt.ieeer9.org/index.php/transactions/article/view/9658

***Index Terms*—Dual-input converter (DIC), Electric Vehicles (EVs), Golden Eagle Optimization (GEO), Hybrid GEO-PO (Golden Eagle Optimization and Puma Optimizer) algorithm, Puma Optimizer (PO), Wireless Power Transfer (WPT).**

NOMENCLATURE

Acronyms

CV	Constant Voltage
DIbB	Dual-Input Buck-Boost Converter
DISO	Dual-Input Single Output Converter
EV	Electric Vehicle
FPGA	Field Programmable Gate Array
GEO	Grey Wolf Optimization
ITAE	Integral Time Absolute Error
PI	Proportional-Integral Controller
PO	Puma Optimizer
MPPT	Maximum Power Point Tracking
MISO	Multi-Input Single-Output
PV	Photovoltaic
WPT	Wireless Power Transfer
ZN	Ziegler Nichols

Symbols

d_1, d_2, d_3	Duty cycles of different switches
$F(\Psi)$	Objective function
i_L, v_C	Inductor current and capacitor voltage
I_{bat}	Battery charging current
I_{PV}, I_{WPT}, I_{PV+WPT}	Currents in PV, WPT systems, and combined PV-WPT input
K_p, K_i	Proportional and integral gains
K_p^*, K_i^*	Optimized controller gains
L, C, R	Inductance, capacitance, and resistance
t_{sim}	Simulation time
U_{ml}	Amplitude of inverter output
V_0, $\tilde{v}_0$	Output voltage and its small-signal variation
V_{PV}, V_{WPT}	PV system voltage and WPT system voltage
V_{ref}	Reference voltage
V_{Rx}, V_{Tx}	Receiver and transmitter coil voltages
V_T	Battery terminal voltage
Ψ	Controller parameter set $\{K_p, K_i\}$
$\tilde{d}_1$, $\tilde{d}_2$, $\tilde{d}_3$	Small-signal duty cycle variations
$\tilde{i}_L$	Small-signal inductor current variation
$\tilde{v}_C$	Small-signal capacitor voltage
$\tilde{v}_{PV}$	Small-signal PV voltage variation
$\tilde{v}_{WPT}$	Small-signal WPT voltage variation

The associate editor coordinating the review of this manuscript and approving it for publication was Diego Rivelino Espinoza Trejo (*Corresponding author: Ganesh Babu Mattaparthi*).

Ganesh Babu Mattaparthi, and S. R. N. Panugothu are with the Department of Electrical and Electronics Engineering, National Institute of Technology, Tiruchirappalli, TN 620015, India (e-mails: 407120053@nitt.edu, and psnayak@nitt.edu).

I. Introduction

THE global transition from Internal Combustion Engine (ICE) vehicles to Electric Vehicles (EVs) is primarily driven by the need for environmental sustainability, energy security, and the depletion of fossil fuel reserves. Governments, industries, and international organizations are actively supporting this shift to reduce greenhouse gas emissions and address climate change challenges. While EVs offer notable advantages such as lower operating costs and zero tailpipe emissions, they also face several challenges, including long charging times, limited charging infrastructure, installation costs, and range anxiety. Most of these challenges can be addressed by developing a robust charging infrastructure [1], integrating onboard renewable energy sources, most likely PV systems along with grid power, as discussed in [2]. Among grid-powered charging techniques [3], plug-in charging is a widely adopted method due to its well-established infrastructure and faster, more efficient energy transfer. However, it is also associated with drawbacks such as cable wear, safety concerns, increased system complexity at high power levels, and interoperability issues. To address these challenges, high-frequency wireless power transfer (WPT)-based charging [4], [5] is emerging as a promising alternative, offering a contactless, automated solution that reduces mechanical wear and enhances user convenience [6]. However, for efficient management of power from such hybrid sources, a multi-input single-output (MISO) DC-DC converter [7] plays an important role in providing efficient EV battery charging by simultaneously utilizing multiple energy sources like PV and WPT. It enhances reliability, ensures a stable output, and supports adaptive control for dynamic input variations.

Among the MISO converters, non-isolated dual-input converters (DICs) are preferred for their high efficiency, compact design, cost-effectiveness, and superior dynamic performance compared to isolated topologies. Numerous dual-input converter (DIC) topologies have been proposed for integrating multiple energy sources in EV charging systems, but each comes with significant limitations. The converters in [8] support only specific modes (buck-boost or individual buck/boost) and lack bidirectional power flow. Although [9] introduced an additional switch to address this issue, it focused solely on storage-to-load energy flow. The design in [10] enabled mode switching and bidirectional transfer using relays and diodes but added mechanical complexity and reduced reliability. A more streamlined topology in [11] eliminated relays and supported all operating modes with bidirectionality, yet it did not address control challenges under variable source conditions such as those from solar PV and WPT. More complex designs, like the coupled inductor-based converter in [12], complicate controller design, while topologies in [13] and [14] are limited to low-voltage applications or cannot merge energy from both sources. These drawbacks underscore the need for a converter that combines compact hardware, operational flexibility, and robust control. The proposed dual-input single-output (DISO) converter meets these needs using a single inductor, three switches, and three diodes to operate in dual-input boost (DIB), dual-input buck (DIBK), and dual-input buck-boost (DIbB) modes. A PI-based controller derived from the converter's small-signal model ensures stable voltage despite source disturbances [15]. The converter design implemented in this work [16] enables efficient, simultaneous integration of WPT and PV sources without relays or complex magnetics, making it highly suitable for real-world EV charging scenarios.

The proposed converter is capable of operating in buck, boost, and buck-boost modes through dedicated control logic. However, it currently utilizes a PI controller with gain values manually tuned based on stability analysis. With the rapid advancement in computational capabilities and the integration of real-time processing in modern embedded systems, it has become both feasible and advantageous to implement advanced optimization algorithms for automatic tuning of controller gains. Such optimization enhances the robustness and adaptability of the control system, particularly under input voltage fluctuations caused by partial shading in PV systems [17] and coil misalignments in WPT systems [18]. As summarized in Table I, most of the literature applies optimization algorithms primarily to single-input single-output (SISO) converter systems. In contrast, the present work introduces a novel hybrid GEO-PO optimization algorithm tailored for a dual-input single-output (DISO) converter integrated with both PV and WPT sources. This unique application demonstrates the proposed converter's superior capability to ensure stable, efficient, and reliable power delivery to the EV battery under dynamic operating conditions.

Building on recent advancements, this study proposes a hybrid GEO-PO (Golden Eagle Optimization and Puma Optimizer) algorithm to optimize control parameters for a non-isolated dual-input single-output (DISO) converter integrated with wireless power transfer (WPT) and rooftop photovoltaic (PV) sources. The hybrid algorithm merges the broad global search ability of the Golden Eagle Optimization (GEO) algorithm [25] with the fine-tuned local exploitation strength of the Puma Optimizer (PO) algorithm [26], resulting in faster convergence and improved control accuracy. The key contributions of this work include:

- Realization of a dual-input converter architecture that adaptively operates in buck-boost mode to accommodate variable power from WPT and PV sources.
- Development of a novel hybrid GEO-PO algorithm for optimal tuning of a multi-stage PI controller based on small-signal modeling of the DISO converter.
- First-time application of this hybrid optimization strategy for regulating a PV-WPT-based EV charging system under dynamic input conditions, enabling robust constant voltage (CV) mode charging.
- Real-time implementation on an FPGA platform to validate the algorithm's practical viability and suitability for intelligent EV charging infrastructure.

A comprehensive transient analysis under varying input voltages confirms the superior dynamic response and robustness of GEO-PO compared to its standalone counterparts and the conventional Ziegler–Nichols method of gain estimation.

This paper is organized as follows: Section II provides a detailed modeling of the proposed dual-input EV charger, incorporating WPT, PV systems, and the hybrid GEO-PO optimization algorithm-based feedback controller design. Section III describes the hardware setup of the system. Section

TABLE I
A COMPARISON OF VARIOUS OPTIMIZATION-BASED CONTROL STRATEGIES FOR DC-DC CONVERTERS IN THE LITERATURE

Paper	Converter Type	Control Strategy Implemented	Optimization Technique	Input Sources	Key Findings	Performance Metrics	Drawbacks
[19] A. Darcy Gnana Jegha et al.	LUO converter	PI controller for BLDC motor using GWO-based MPPT	Grey Wolf Optimizer (GWO)	Solar PV	Low switching losses, soft start, and high efficiency under low irradiance	Output voltage	Sensitive to motor torque; reliability concerns
[20] Mohan Appikonda et al.	Dual-input boost	Dual-loop control (P & I)	Classical tuning	Renewable sources	Effective small-signal-based control with improved MPPT	MPPT efficiency	Control complexity due to non-minimum phase nature
[21] Ali Mamizadeh et al.	Boost converter	PI controller gain optimization	Cuckoo Optimization Algorithm (COA)	Solar, Wind	COA-based PI controller yields better transient performance	Integral of Absolute Error (IAE)	Dependent on algorithm tuning parameters
[22] S. Rajasekaran et al.	Modified SEPIC (MSEPIC)	PID controller tuned using NSGA-II/INSGA-II	NSGA-II/INSGA-II	Solar PV	98.57% efficiency; better than PSO	Voltage gain, ripple, efficiency	Limited voltage gain and lower conversion efficiency at times
[23] Mehmet Hakan Demir et al.	Buck converter	PSO-based intelligent PID and I controllers	Particle Swarm Optimization (PSO)	PEM Fuel Cell	High path/voltage tracking and energy efficiency	Integral of Time Absolute Error (ITAE)	No hardware validation; simulation only
[24] Ali Ahmad et al.	VSC (Voltage Source Converter)	Vector control with inner current and outer power PI controllers	Ant Colony Optimization (ACO)	Photovoltaic system	ACO improves transient response and disturbance rejection	Integral of Time Absolute Error (ITAE)	No statistical validation; renewables not fully integrated

IV presents the performance analysis based on the proposed feedback controller, including a transient response evaluation and a comparative analysis of the proposed algorithm with its parent algorithms and the Ziegler–Nichols (ZN) method. Section V concludes the paper.

II. HYBRID GEO-PO BASED PI CONTROLLER DESIGN

A. Modeling of PV-WPT Sources fed Dual-Input EV Charger

Dual-input sources here refer to the integration of renewable energy systems into EV charging setups. An EV charger with dual inputs might draw power from both the electrical grid and renewable sources such as solar panels or wind turbines. This setup allows the charger to utilize renewable energy when available, reducing the environmental impact of the charging process. In this design, a dual-input on-board EV charger is proposed, with WPT serving as the primary energy source and a rooftop solar PV panel mounted on the vehicle acting as the secondary source. The block diagram and schematic of the proposed dual-input EV charger are shown in Figs. 1a and 1b, respectively. The modeling of the input sources and the on-board EV charger is described in detail below.

1) PV System: The PV system can be installed either on the rooftops of vehicles or on parking shelters to capture sunlight and convert it into electrical energy. The basic equivalent circuit of a photovoltaic (PV) module, based on the single-diode model, is shown in Fig. 2. This equivalent circuit includes key components such as a photocurrent source, a diode, and resistive elements, among others.

The total current (I_{PV}) and voltage (V_{PV}) are supplied to the EV charger. In the solar module, the photocurrent (Iph), diode current (I_d), and the currents through the series and shunt resistances (I_{PV} and I_{sh}, respectively) are represented by Equations (1) and (2).

$$\begin{cases} I_{PV} = I_{ph} - I_d - I_{sh} \\ I_{ph} = I_L \left(1 - \dfrac{T}{T_{ref}}\right) \\ I_d = I_o \left(e^{\frac{qV_d}{nkT}} - 1\right) \\ I_{sh} = \dfrac{V_{PV} + I_{PV} R_s}{R_{sh}} \end{cases} \tag{1}$$

$$V_{PV} = \left(\frac{kTN_S}{q}\right) \times \ln\left(\left(\frac{I_L}{I_0}\right) + 1\right) \tag{2}$$

Here, I_L represents the light-generated current, I_s is the reverse saturation current, q is the charge of an electron, and V_{PV} is the voltage across the solar cell. Additionally, n is the ideality factor, k is the Boltzmann constant, T is the operating temperature, T_{ref} is the reference temperature, R_s is the series resistance, and R_{sh} is the shunt resistance. V_{PV} is the voltage output of the PV system fed to the DIbB converte and C_{pv} is the parallel capacitor to eliminate high frequency components in the PV system into the converter input.

2) WPT System: Wireless power transfer (WPT) is an emerging technology used to transfer electrical energy from a transmitter to a receiver without physical connections, utilizing various methods and technologies that rely on time-varying electric, magnetic, or electromagnetic fields. In the system, the rectified grid source is fed to the inverter through a DC link. The inverter converts the DC power into high-frequency AC, which is then supplied to the transmitter coil via a compensation network. The high-frequency AC received by the compensated receiver coil is rectified and delivered to

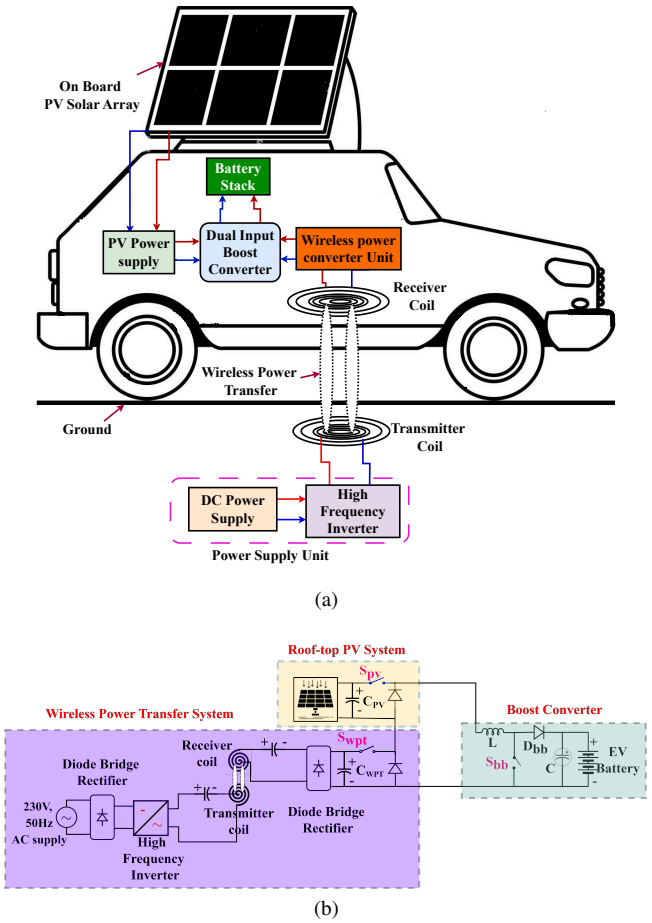

Fig. 1. Dual-input EV charger. (a) Block diagram of the dual-input charging system. (b) Schematic Diagram of the Dual-Input On-board EV charger.

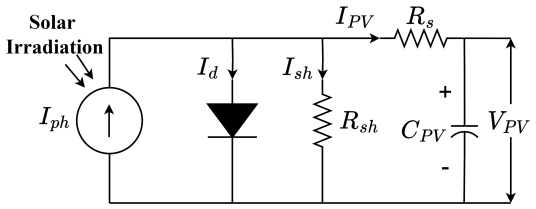

Fig. 2. Equivalent circuit of PV cell.

the EV charger. The power flow diagram and basic circuit model of the WPT system with S-S compensation are shown in Fig. 3a and 3b respectively. To enhance active power transfer, series-series (S-S) compensation is applied, where two external capacitors, C_1 and C_2, are connected in series with the primary and secondary windings of the system. This configuration improves the overall efficiency and performance of the WPT system. The series–series (S–S) compensated high-frequency AC signal from the receiver coil (Rx) is passed through a filter capacitor (C_{wpt}) before entering the DISO converter. This capacitor effectively attenuates high-frequency components and minimizes voltage ripple, ensuring a smoother DC input for the converter.

Here, the WPT system model is modeled through equations below:

As shown in Fig. 3b, U_1 is high frequency single phase inverter output fundamental RMS voltage and is given by Equation (3).

$$U_1 = \frac{2\sqrt{2}}{\pi} U_{ml} \tag{3}$$

Where, U_{ml} is the amplitude of the high frequency single phase inverter whose output has a rectangular voltage profile. The loop currents analysis is given below, and the WPT system model is represented through Equations (4) - (6) as shown below.

$$-u_1 + \frac{1}{C_1}\int_0^t i_1 dt + u_{c_1}(0) + R_1 i_1 + L_1 \frac{di_1}{dt} + M\frac{di_2}{dt} = 0 \tag{4}$$

$$-L_2\frac{di_2}{dt} + M\frac{di_1}{dt} + R_2 i_2 - \frac{1}{C_2}\int_0^t i_2 dt - u_{C_2}(0) - R_z i_2 = 0 \tag{5}$$

$$\begin{bmatrix} I_{S_1} \\ I_{S_2} \end{bmatrix} = \begin{bmatrix} R_1 + j\left(\omega L_1 - \frac{1}{\omega C_1}\right) & -j\omega M \\ -j\omega M & R_2 + R_Z + j\left(\omega L_2 - \frac{1}{\omega C_2}\right) \end{bmatrix} \times \begin{bmatrix} \tilde{i}_L \\ \tilde{v}_c \end{bmatrix} \tag{6}$$

The receiver output voltage (U_2) is given by,

$$U_2 = j\omega M I_{S_1} + R_2 I_{S_2} + I_{S_2}\left(-j\omega L_2 + \frac{j}{\omega C_2}\right) \tag{7}$$

The diode bridge rectified output voltage (i.e., V_{wpt}) is given by,

$$V_{wpt} = \frac{2\sqrt{2}U_2}{\pi} \tag{8}$$

3) Dual Input EV Charger Operation: The equivalent circuit diagram of the proposed dual-input on-board EV charger is shown in Fig. 4a. The input sources, PV and WPT, are connected to a DISO converter, which can operate in various configurations such as buck, boost, and buck-boost, depending on the control logic and switching pulses given to the switches. However, this paper focuses solely on the dual-input buck-boost configuration to ensure that the input sources provide the required rated voltage for EV charging. The modes of operation for the buck-boost configuration are depicted in Figs. 4b-4e, with the corresponding timing diagram in Fig. 4f.

The switching patterns for the different modes of operation are outlined in Table II. Upon analyzing the circuit diagrams corresponding to the various modes of operation, it is observed that Modes I, II, and III resemble the ON-state of a conventional single-input single-output (SISO) buck-boost converter, while Mode IV corresponds to the OFF-state. Therefore, the converter in this configuration can be effectively interpreted as a fundamental buck-boost converter with dual-input capability.

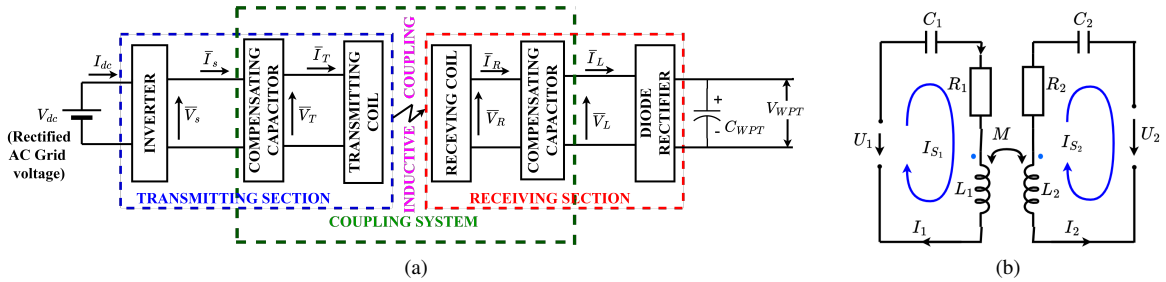

Fig. 3. (a) Power flow block diagram of the WPT system. (b) Simplified circuit with series–series compensation and loop current analysis.

TABLE II
SWITCHING PATTERN OF THE DUAL-INPUT CONVERTER FOR DIFFERENT MODES OF OPERATION AS A BUCK–BOOST CONVERTER

Mode	S_{PV}	D_{PV}	S_{WPT}	D_{WPT}	S_{BB}	D_{BB}
Mode I	ON	OFF	OFF	ON	ON	OFF
Mode II	ON	OFF	ON	OFF	ON	OFF
Mode III	OFF	ON	ON	OFF	ON	OFF
Mode IV	OFF	ON	OFF	ON	OFF	ON

B. Mathematical Modeling of the Converter

The state-space model of Dual input Buck Boost (DIbB) converter is given below.

$$\begin{bmatrix} L & 0 \\ 0 & C \end{bmatrix} \begin{bmatrix} \tilde{i}_L \\ \tilde{v}_c \end{bmatrix} = \begin{bmatrix} 0 & -1+(d_1+d_2+d_3) \\ 1-(d_1+d_2+d_3) & \frac{-1}{R} \end{bmatrix} \begin{bmatrix} \tilde{i}_L \\ \tilde{v}_c \end{bmatrix} + \begin{bmatrix} d_1+d_3 & d_2+d_3 \\ 0 & 0 \end{bmatrix} \begin{bmatrix} \tilde{v}_{PV} \\ \tilde{v}_{WPT} \end{bmatrix} + \begin{bmatrix} V_{PV}+V_C \\ -I_L \end{bmatrix} \tilde{d}_1 + \begin{bmatrix} V_{WPT}+V_C \\ -I_L \end{bmatrix} \tilde{d}_2 + \begin{bmatrix} V_{PV}+V_{WPT}+V_C \\ -I_L \end{bmatrix} \tilde{d}_3 \tag{9}$$

$$C\frac{dV_C}{dt} = (1-d_1-d_2-d_3)\,\tilde{i}_L - \frac{1}{R}\tilde{v}_c - I_L\tilde{d}_1 - I_L\tilde{d}_2 - I_L\tilde{d}_3 \tag{10}$$

Similarly the Equation (9) to form output equation as below,

$$\begin{aligned} v_o &= -v_c; i_1 = d_1\tilde{i}_L + I_L\tilde{d}_1; \\ i_2 &= d_2\tilde{i}_L + I_L\tilde{d}_2; i_3 = d_3\tilde{i}_L + I_L\tilde{d}_3 \end{aligned} \tag{11}$$

The proposed system equivalent small signal modal circuit is shown in Fig. 5, and the transfer function of the small signal model of the proposed system is given below:

$$\frac{\tilde{v}_C(s)}{\tilde{d}_1(s)} = \frac{[1-(d_1+d_2+d_3)]\,(V_{PV}+V_C) - sLI_L}{s^2LC + s\frac{L}{R} + [1-(d_1+d_2+d_3)]^2} \tag{12}$$

$$\frac{\tilde{v}_C(s)}{\tilde{d}_2(s)} = \frac{[1-(d_1+d_2+d_3)]\,(V_{WPT}+V_C) - sLI_L}{s^2LC + s\frac{L}{R} + [1-(d_1+d_2+d_3)]^2} \tag{13}$$

$$\frac{\tilde{v}_C(s)}{\tilde{d}_3(s)} = \frac{[1-(d_1+d_2+d_3)]\,(V_{PV}+V_{WPT}+V_C) - sLI_L}{s^2LC + s\frac{L}{R} + [1-(d_1+d_2+d_3)]^2} \tag{14}$$

The inputs to this model include three duty cycles, d_1, d_2 and d_3, along with the source voltages V_{PV} and V_{WPT}. The duty cycles are adjusted by the PI controller. The model evaluates the converter's output voltage V_o (i.e., V_T), compares it to the rated voltage, and computes the error, which is then fed into the PI controller. The PI controller calculates the necessary adjustments to the duty cycles $\tilde{d}_1$, $\tilde{d}_2$, and $\tilde{d}_3$. The initial values for the duty cycles, d_{01}, d_{02} and d_{03}, are carefully chosen to ensure optimal performance.

C. Problem Formulation

The block diagram of the EV battery charger with a PI controller is illustrated in Fig. 6. The objective is to determine the optimal values for K_p and K_i to ensure the output voltage of the EV charger remains constant throughout the battery charging process. If V_{ref} is the rated output voltage of the charger and V_o is the instantaneous output voltage, constant voltage charging can be achieved by maintaining V_o equal to V_{ref}. Let the error be defined as $(e) = V_{\text{ref}} - V_o$, representing the difference between the rated and actual output voltages of the charger. The goal is to find the optimal values for the controller constants K_p and K_i that minimize this error. This task can be formulated as an optimization problem, as shown in Equation (15), with the objective to minimize the error subject to certain constraints.

$$F(\Psi) = \int_0^{t_{\text{sim}}} t \cdot |V_{\text{ref}} - V_o|\, dt \tag{15}$$

$$\Psi_{(lower)} \leq \Psi \leq \Psi_{(upper)}$$

where, t_{sim} = simulation time, t = Structural Interval and, Ψ = K_p, K_i in the controller structure.

It may be noted that the minimum and maximum values of K_p and K_i are obtained using the small signal model developed in Equations (12) - (14) and their stability analysis.

D. PI Controller Parameter Optimization using Hybrid GEO-PO Algorithm

The Hybrid GEO-PO optimization algorithm combines the strengths of the Golden Eagle Optimizer (GEO) and the Puma Optimizer (PO), creating a versatile and efficient optimization framework. GEO, inspired by the hunting strategies of golden eagles, emphasizes robust global exploration, while PO, based on the territorial and predatory behavior of pumas, excels in fine-tuned local exploitation. This synergy allows the hybrid algorithm to leverage GEO's strong exploration capabilities,

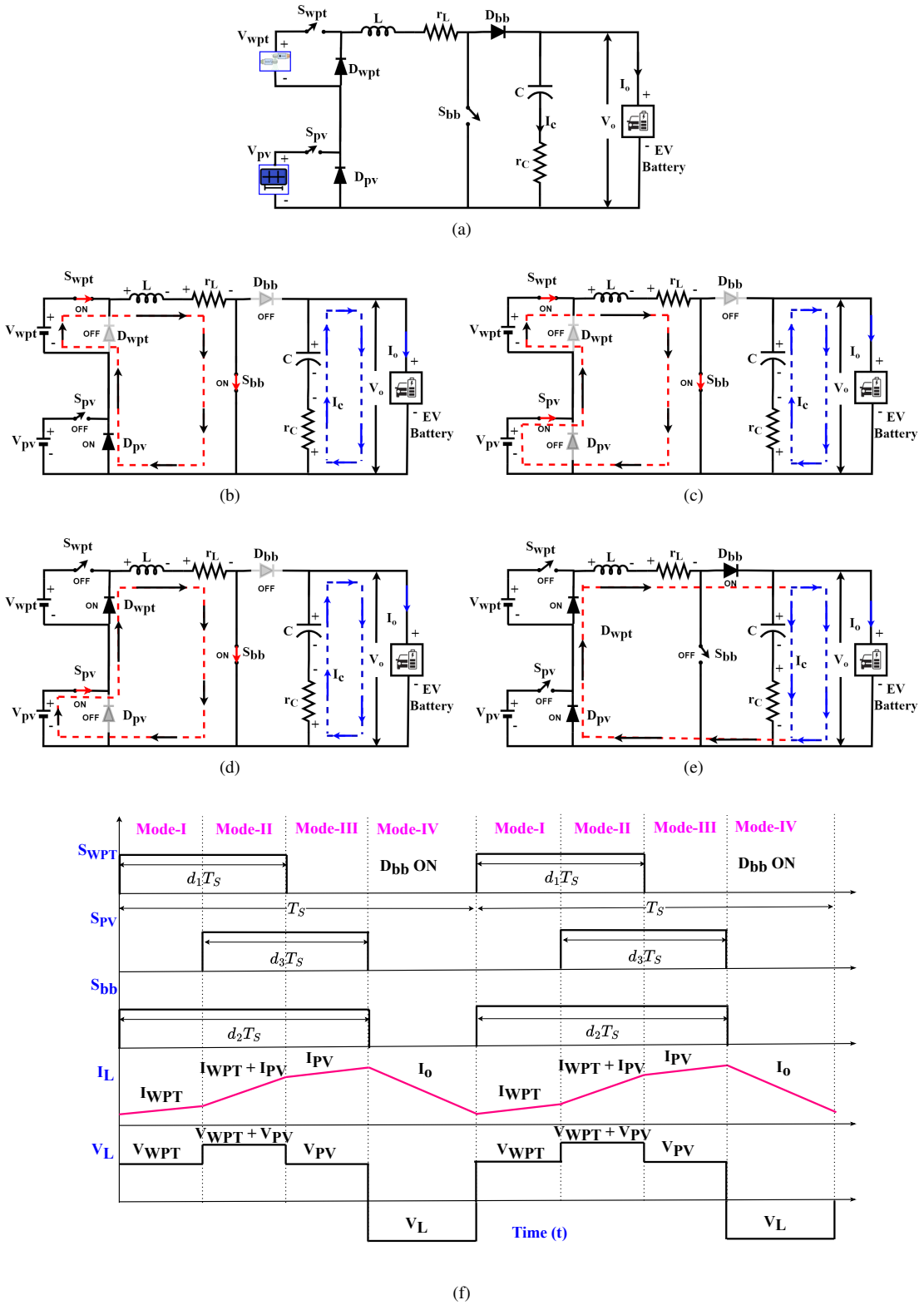

Fig. 4. (a) Overall circuit diagram of Dual input converter. (b) Mode-I operation. (c) Mode-II operation. (d) Mode-III operation. (e) Mode-IV operation. (f) Timing diagram of Dual-Input converter operating as buck-boost converter.

significantly reducing the likelihood of being trapped in local optima during the early search phase. Simultaneously, PO's precise exploitation mechanisms enhance convergence speed in the later optimization stages.

By integrating these complementary characteristics, the hybrid GEO-PO algorithm achieves a superior balance between exploration and exploitation, resulting in improved robustness and adaptability across diverse and multi-modal optimization

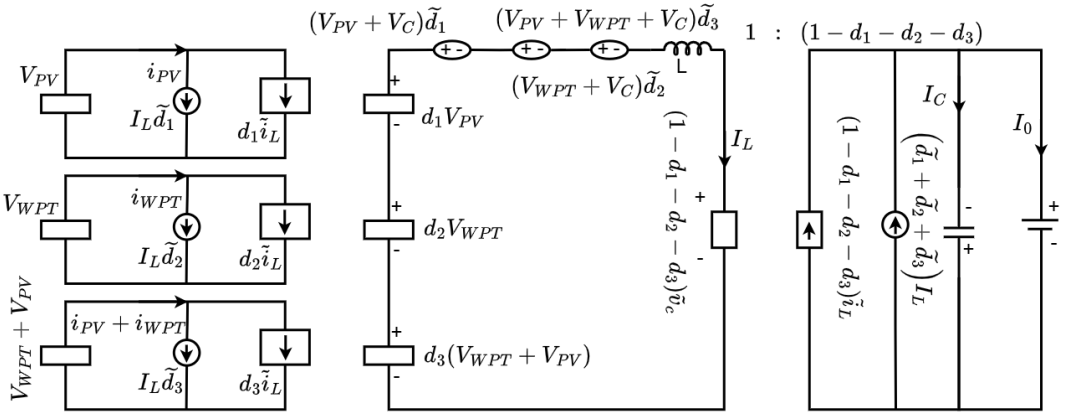

Fig. 5. Proposed system equivalent small signal model circuit.

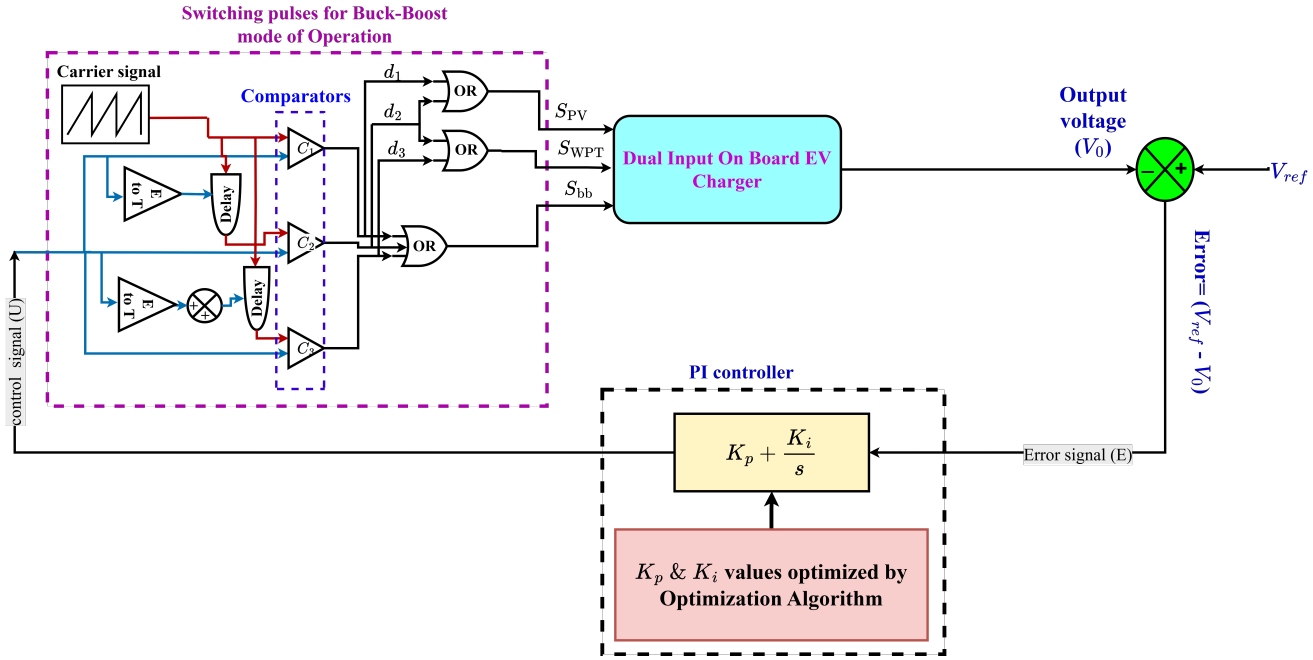

Fig. 6. Block diagram of the DIC on-Board EV charger with Controller.

landscapes. Hence application of this hybrid algorithm to the current problem of optimizing the PI gains of the proposed DISO converter is shown in clear steps in Algorithm 1. Various steps in the proposed method of control and detailed usage of the proposed algorithm for optimizing the PI controller gains of a Dual-input converter for input voltage variations is shown in the Fig. 7.

III. Hardware Description

The experimental setup consists of a PV system, a WPT system, and a dual-input on-board EV charger, which includes capacitors, diodes, and an inductor for buck and boost operations. For this work, a solar emulator (SM100-AR-75 model) is used to simulate the PV system. This emulator can adjust various voltage levels and current limits within the ranges of 0-100V and 0-16A, respectively. It features digital constant voltage (CV) and constant current (CC) settings, an Ethernet interface with 100 Mb/s speed and full-duplex communication through an RJ45 connector, high voltage isolation, and a USB port for exchanging input and output settings and waveforms.

The WPT power source includes an H-bridge inverter, a compensation topology, coupled coils, and a receiver-side rectifier. The H-bridge inverter uses SCH2080KE N-channel SiC power MOSFETs rated at 1200V and 40A, with a maximum frequency of 1 MHz, to deliver high-frequency AC power to the coupled coils. The coils are wound with Litz wire (1000 strands) in a square shape, with inner and outer diameters of 4 cm and 36 cm, respectively. The self-inductance of both the transmitter and receiver coils is measured at 0.177 mH. To compensate for the inductance of the coils, a polarized capacitor bank with a total capacitance of 18.75 nF (comprising eight 0.15 µF capacitors connected in series) is used. The full-bridge rectifier is implemented with an MUR30120 ultra-fast recovery rectifier.

The dual-input converter is equipped with SKM 75GB063D super-fast NPT-IGBT modules, which have a voltage rating of 600V and a current rating of 100A. The input inductor is an iron-core type with 5 mH inductance and a 40A rating, while the output capacitor is an electrolytic type with 2200

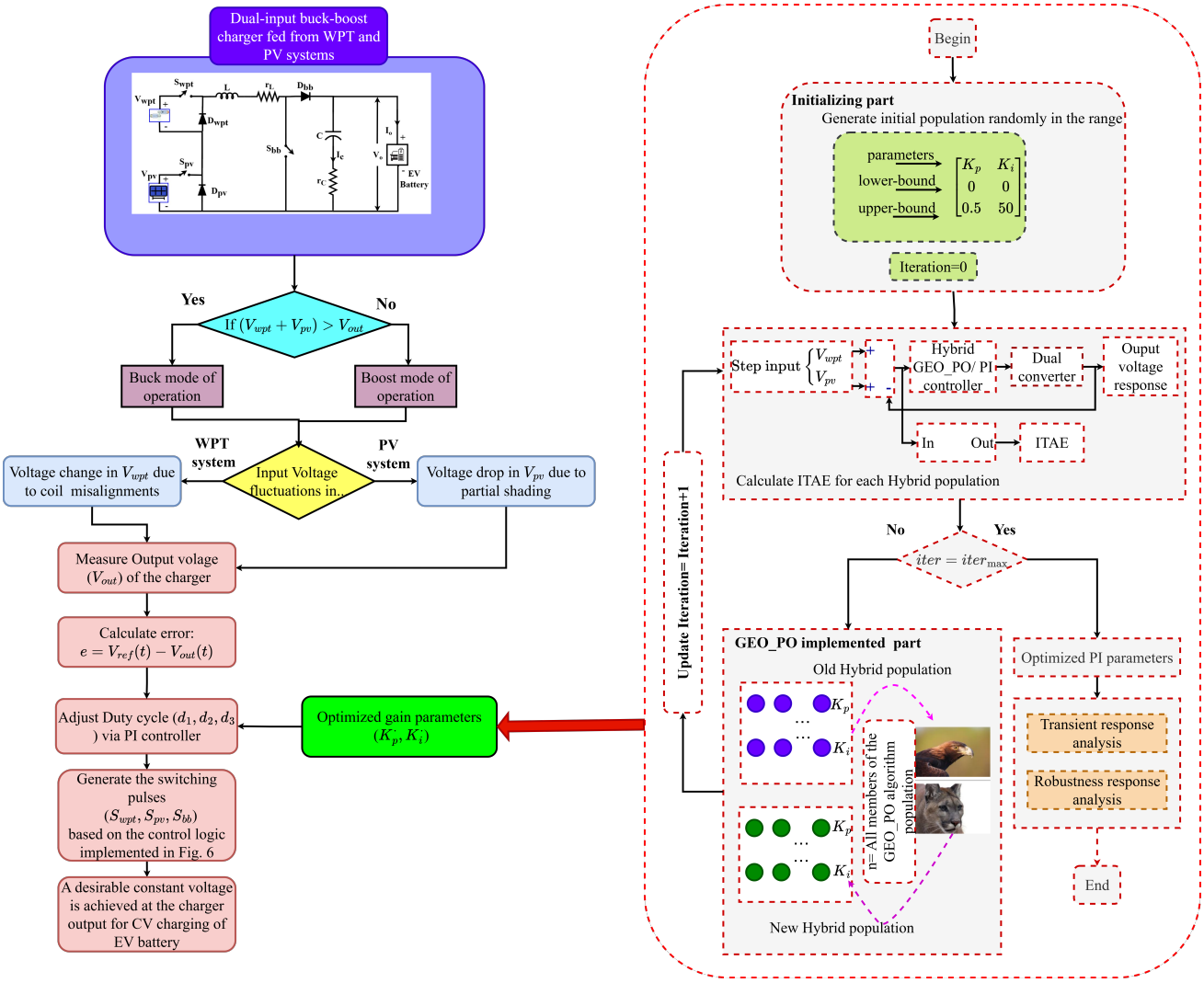

Fig. 7. The schematic of the control action that uses the Hybrid GEO-PO optimization method to generate the optimized gain values to regulate the output voltage of a Dual-input converter.

μF capacitance and a maximum DC voltage of 450V. The EV battery bank is designed for a full charge voltage of 71V, consisting of five 12V, 6AH, 75Wh LiFePO4 batteries connected in series.

To measure the input and output currents, a Hall effect current sensor (HE055T01) is used, and voltages are sensed using the IC7440. The sensed voltage and current values are amplified by four AD8022 operational amplifiers with two analog inputs. These signals are then converted to digital using a simultaneous sampling SAR ADC (AD7366). The digital signals are processed by an FPGA controller (SPARTAN-6 XC6SLX9). PWM pulses are generated by a XILINX XC2C258 complex programmable logic device, and the CY7C68013A USB microcontroller, used in conjunction with the FPGA development board, provides USB capability to the system. Logical code is uploaded to the FPGA board using the XILINX ISE design suite through a JTAG cable. The overall hardware setup is depicted in Fig. 8.

IV. Results and Discussion

A custom MATLAB program has been developed for designing the feedback controller using the Hybrid GEO-PO algorithm. The parameters for the GEO-PO algorithm were determined through trial and error, since GEO-PO is a population-based optimization technique, Fig. 9 shows the evolution of the objective function value for the best control parameters over iterations. The convergence is rapid, with the objective function value (ITA error) reaching as low as 0.000695 after 30 iterations compared to the GEO, PO algorithms and ZN method gain estimation. Consequently, the optimized feedback controller constants are found to be K_p^* = 0.188 and K_i^* = 31.97 following these 30 iterations and the optimized gain values of the parent algorithms with their algorithmic specific data is presented in Table III.

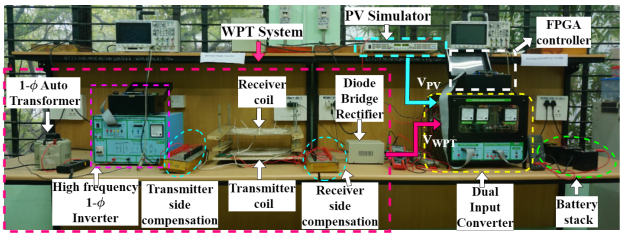

Fig. 8. Hardware setup of the dual-input on-board EV charger.

Algorithm 1 Hybrid GEO-PO Algorithm for Optimizing PI Controller Gains

Initialize Parameters: Set maximum iterations $t_{\max}$, population size N, GEO exploration weight α_{GEO}, PO exploitation factor α_{PO}, and convergence tolerance ϵ.
Initialize Population: Randomly initialize each agent's position representing PI controller gains (K_p, K_i) within bounds.
Evaluate Fitness: For each agent, simulate the DC-DC converter using (K_p, K_i) and calculate the ITA error as:

$$ITAE = \int_0^T |V_{\text{ref}}(t) - V_{\text{out}}(t)| \cdot t \, dt$$

$V_{\text{ref}}(t)$: Desired reference output voltage.
$V_{\text{out}}(t)$: Actual converter output voltage.
t: Time variable used to penalize errors occurring later.
T: Total simulation time.

Store Best Solution: Identify and store the (K_p, K_i) values with the lowest ITA error as x_{best}.
while termination criteria not met **do**
  Exploration Phase (GEO):
  for each agent i in the population **do**
    Calculate the distance vector d_i between agent i and x_{best}.
    Update position based on GEO exploration:

$$x_{\text{new}} = x_{\text{best}} + \alpha_{\text{GEO}} \cdot r_1 \cdot d_i + r_2 \cdot \sin(2\pi r_3) \cdot d_i$$

r_1: Controls magnitude of linear exploration ($r_1 \in [0, 1]$)
r_2: Scales sinusoidal perturbation ($r_2 \in [0, 1]$)
r_3: Determines oscillation frequency ($r_3 \in [0, 1]$)

    Evaluate Fitness of x_{new}:
    1) Simulate the DC-DC converter with updated (K_p, K_i).
    2) Calculate ITA error as the fitness for x_{new}.
    if new fitness is better **then**
      Update agent's position: $x_i = x_{\text{new}}, \quad f_i = f_{\text{new}}$
    end if
  end for
  Exploitation Phase (PO):
  for each agent i in the population **do**
    Update position based on PO exploitation:

$$x_{\text{new}} = x_{\text{best}} + \alpha_{\text{PO}} \cdot r_4 \cdot d_i + r_5 \cdot \text{randn}() \cdot d_i$$

r_4: Scales deterministic step toward best solution ($r_4 \in [0, 1]$)
r_5: Scales local Gaussian noise ($r_5 \in [0, 1]$)
randn(): Standard normal distribution noise ($\mu = 0$, $\sigma = 1$)

    Evaluate Fitness of x_{new}:
    1) Simulate the DC-DC converter with updated (K_p, K_i).
    2) Calculate ITA error as the fitness for x_{new}.
    if new fitness is better **then**
      Update agent's position: $x_i = x_{\text{new}}, \quad f_i = f_{\text{new}}$
    end if
  end for
  Update Best Solution: If any x_{new} has a better ITA error than x_{best}, update x_{best}.
  Update GEO and PO weights α_{GEO} and α_{PO} dynamically, if required.
end while
Return x_{best} as the optimal (K_p, K_i) values.

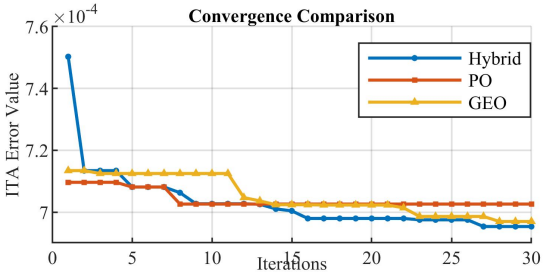

Fig. 9. Convergence graph of the Proposed algorithm along with GEO and PO algorithms.

The FPGA-based dual-input on-board EV charger, as shown in Fig. 1b, was developed in the laboratory for the purpose of charging the EV battery at a constant voltage. Waveforms were recorded during testing, and the measured results are presented

TABLE III
OPTIMIZATION PARAMETERS AND RESULTS FOR GEO, PO, HYBRID GEO-PO, AND ZN METHOD

Parameter	GEO	PO	Hybrid GEO-PO	ZN Method
Exploration Factor (α)	2	–	2	–
Exploitation Factor (β)	1.5	–	1.5	–
Exploitation Weighting Factor (γ)	–	0.5	Starts at 0.5, increases by 5% per iteration	–
Random Factor 1 (r_1)	Uniform random [0, 1]	Uniform random [0, 1]	Uniform random [0, 1]	–
Random Factor 2 (r_2)	Uniform random [0, 1]	Uniform random [0, 1]	Uniform random [0, 1]	–
Population Size	30	30	30	–
Number of Variables (K_p, K_i)	2	2	2	–
Number of Iterations	30	30	30	–
Optimized Control Parameters (K_p^*, K_i^*)	[0.1038, 9.0486]	[0.0607, 4.3252]	[0.1882, 31.9676]	[0.24, 20.07]
ITAE Error	0.000696989	0.000702615	0.000695364	0.001876654

alongside the simulation results, covering various cases based on the connected input sources. The analysis considers several parameters, including V_{WPT} (input voltage from the WPT system to the DIbB converter), V_{PV} (input voltage from the PV system to the DIbB converter), V_T (terminal voltage of the DIbB converter), I_{bat} (output current of the DIbB converter, or the EV battery charging current), V_{Rx} (receiver coil voltage), and I_{Rx} (receiver coil current).

A. Performance Analysis of the Dual-Input EV Charger

1) Case-I (No change in the Input, Output Parameters): The operation of the proposed EV charger, utilizing the control parameters optimized through the Hybrid GEO-PO algorithm, is demonstrated while charging the EV battery at a regulated constant voltage of 71V. This is achieved under optimal operating conditions, where the WPT system features a perfectly aligned transmitter (Tx) and receiver (Rx) coil configuration. The alignment ensures a stable WPT receiver voltage (V_{WPT}) of 120V, facilitating efficient power transfer. Additionally, the PV system, comprising four solar panels connected in series each rated at 12V delivers a consistent PV string voltage (V_{PV}) of 48V.

The input voltages to the DIbB converter, along with the corresponding EV battery charging voltage and current profiles, are depicted in Fig. 10a. These results highlight the stable and effective performance of the proposed charging system. Furthermore, the high-frequency voltage (V_{Rx}) and current (I_{Rx}) waveforms at the receiver coil of the WPT system are presented in Fig. 10b, illustrating the dynamic characteristics of the resonant wireless energy transfer mechanism for optimal power flow from both WPT and PV sources.

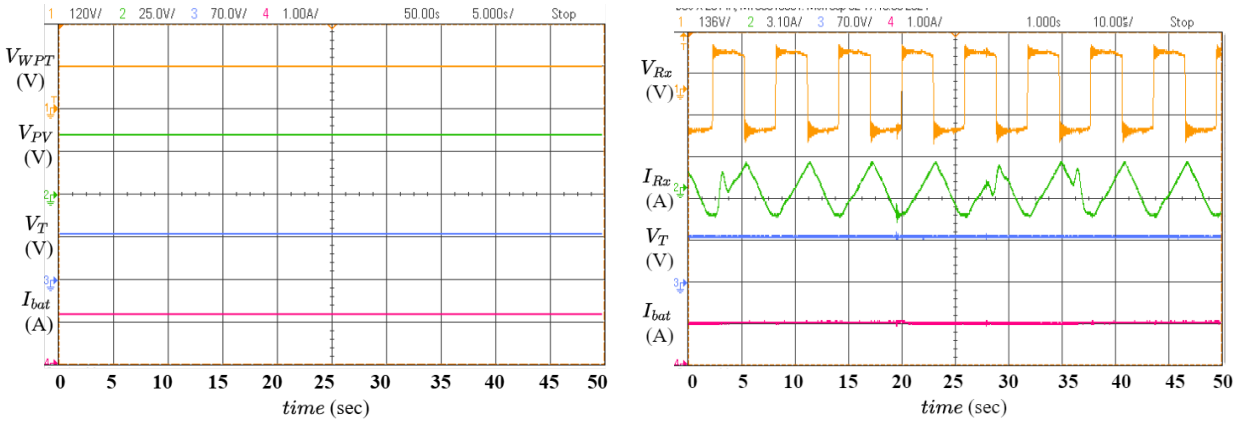

Fig. 10. (a) Voltage and Current Waveforms during No step change in input parameters. (b) WPT system Receiver voltage (V_{Rx}) and current (I_{Rx}).

2) Case- II (Step change in the WPT Input to Converter): In this scenario, the stable operating charger described in *Case-I* is subjected to various Rx coil misalignments, as illustrated in Fig. 11, leading to significant variations in the WPT receiver voltage (V_{WPT}). Despite these disturbances, the controller demonstrates its effectiveness in managing the charging current and maintaining stable operation. An in-depth analysis of the system's behavior is presented in Fig. 12, with the performance categorized into distinct regions based on the type of misalignment. In *Region-1*, the Rx coil is subjected to angular misalignment, where the plane of the Rx coil is tilted relative to the Tx coil by an angle of $5.7°$, causing the receiver voltage to increase from 120V to 170V. Similarly, in *Region-2*, a combination of planar and angular misalignments featuring a 7 cm planar displacement and an angular tilt of $5.7°$ further increases the receiver voltage to 210V.

In *Region-3*, the Rx coil is subjected solely to planar misalignment with a 7 cm displacement, leading to a reduction in the receiver voltage from 210 V to 170 V. Across all these scenarios, the Hybrid GEO-PO algorithm-based controller ensures effective regulation of the converter output voltage, maintaining a constant and reliable charging voltage for the EV battery. This highlights the controller robust adaptability to misalignment-induced disturbances. A comprehensive transient analysis of the system's performance under these conditions for proposed algorithm with its parent algorithms and ZN method is detailed through a bar graph as shown in the Fig. 13a, and the relative improvement in the transient response compared to other methods is also shown in the Fig. 13b offering valuable insights into the control action and dynamic response across the identified regions.

3) Case-III (Step change in the PV Input to Converter): In this scenario, the wireless power transfer (WPT) system maintains a constant output voltage, assuming perfect alignment between the transmitter (Tx) and receiver (Rx) coils. The secondary power source, a 48 V photovoltaic (PV) system, supplies power to the electric vehicle (EV) battery. However, the PV system is subjected to varying partial shading conditions, which cause fluctuations in its output voltage. These voltage

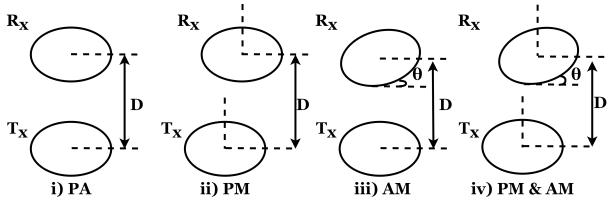

Fig. 11. Various Misalignments between the transmitter receiver coils in WPT system (i) Perfectly aligned (PA) (ii) Planar Misalignment (PM) (iii) Angular Misalignment (AM) (iv) Planar & Angular Misalignment (PM & AM

variations, in turn, influence the output voltage of the dual-input converter. To mimic these shading conditions, a solar emulator is used to simulate the voltage changes. The proposed controller, whose gain parameters are optimized using the proposed Hybrid GEO-PO algorithm, effectively ensures the system voltage remains stable despite these variations.

A comprehensive analysis is presented in terms of different operating regions, as illustrated in Fig. 14. In *Region-1*, one of the 12V PV panels in the system experiences partial shading, resulting in the bypassing of this panel and causing the system voltage to drop from 48V to 36V. This transient voltage dip is effectively controlled by the proposed algorithm. In *Region-2*, partial shading affects two 12V panel, which are subsequently disconnected, further reducing the PV system voltage from 36V to 24V. Finally, in *Region-3*, one of the bypassed panels is reconnected, leading to a sudden increase in the system voltage from 24V back to 36V. Throughout all these fluctuations, the proposed controller successfully maintains a constant output voltage, despite the variations in input voltage.

A detailed analysis of the transient behavior of the charging current in these regions is presented in the form of a bar graph as shown in the Fig. 15a, providing further insights into the proposed controller's performance under dynamic shading conditions, also a comprehensive performance comparison graph illustrating various metrics of the proposed hybrid algorithm against its parent algorithms (GEO and PO) as well as the conventional ZN method is presented in Fig. 15b.

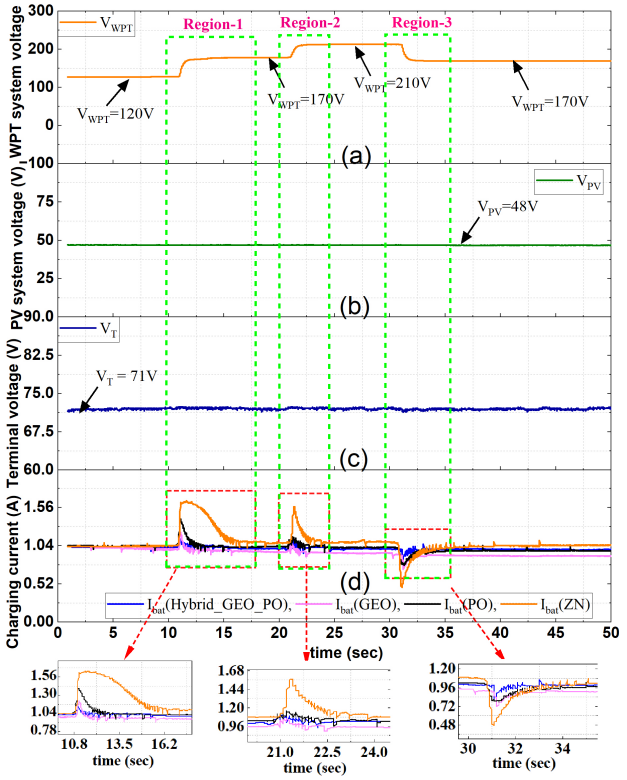

Fig. 12. Voltage and Current Waveforms during step change in WPT voltage. (a) WPT system receiver voltage. (b) PV system voltage. (c) Terminal voltage of the charger. (d) Battery charging current.

V. Conclusions

This paper presents the design and analysis of a feedback controller for a dual-input single-output (DISO) on-board EV charger, optimized using a Hybrid GEO-PO algorithm. The charger operates with two complementary energy sources: photovoltaic (PV) and wireless power transfer (WPT) systems. The proposed controller maintains a constant output voltage during the charging process supporting the constant voltage (CV) mode of charging of the EV battery and ensures stable operation under varying input conditions.

Charging performance was assessed by analyzing transient responses of current and voltage under step changes in input. The PI controller gains, optimized via the proposed hybrid algorithm, showed reliable performance in constant voltage (CV) mode. Under WPT voltage fluctuations caused by transmitter–receiver misalignments, the controller was compared with those optimized by standalone GEO, PO algorithms, and the Ziegler–Nichols method. The Hybrid GEO-PO algorithm consistently delivered superior performance with faster settling times, lower overshoot, and improved transient response.

The results underscore the effectiveness of the Hybrid GEO-PO approach in enhancing the responsiveness and robustness of EV chargers. However, potential limitations include performance degradation due to unmodeled nonlinearities, parasitic effects, and environmental variations such as temperature or component aging. The inherent electrical inertia of IPT-based WPT systems may delay dynamic response, and the optimization's sensitivity to algorithmic parameters, along with unmodeled real-time issues like signal noise and hardware delays, could affect system stability. Overall, the proposed

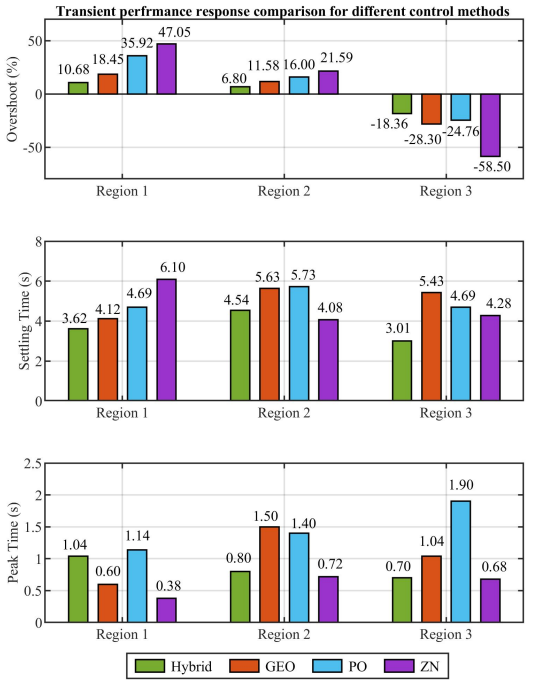

(a)

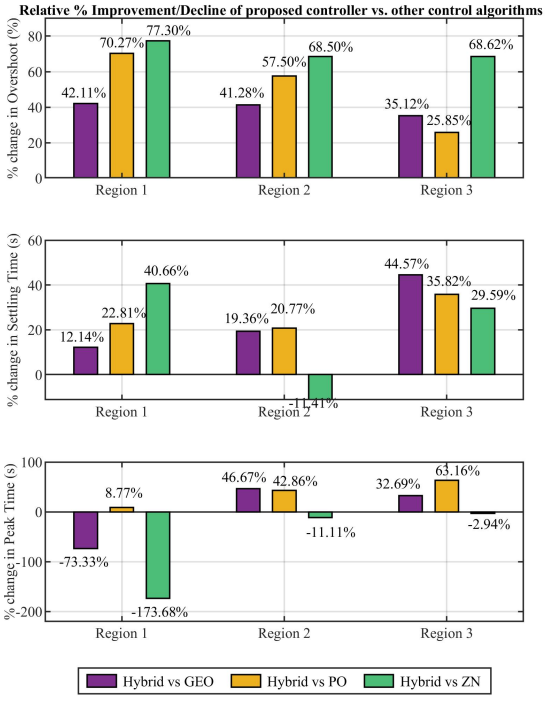

(b)

Fig. 13. (a) Transient Response Performance for WPT step voltage changes: Proposed Hybrid GEO-PO algorithm vs. parent algorithms & ZN method. (b) Transient Response improvement of proposed GEO-PO algorithm vs. parent algorithms & ZN method for WPT system voltage changes.

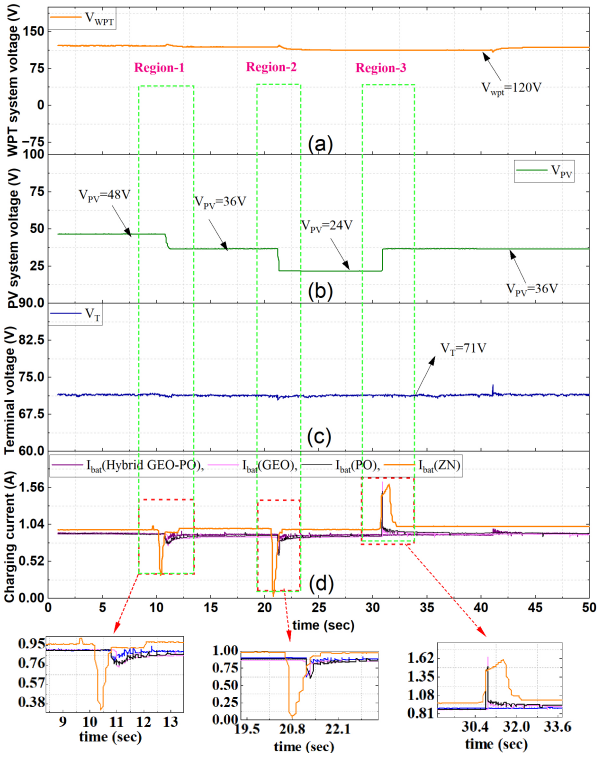

Fig. 14. Voltage and Current Waveforms during step change in PV voltage. (a) WPT system receiver voltage. (b) PV system voltage. (c) Output voltage of the charger. (d) Battery charging current.

method supports efficient, reliable, and stable charging in next-generation EV systems integrating PV and WPT sources.

VI. Appendix

The specifications of the WPT system, Roof-top PV system and the Dual-input converter are specified as below,

1. WPT System: Wire type: Litz, Coil turns: 28, Frequency: 85 kHz, Self-inductance: 177 µH, Capacitor: 18.75 nF, Length: 36 cm, Width: 36 cm.
2. Rooftop PV System: Technology: cSi, Power (STC): 100 W, Max. power voltage (V_{mpp}): 48.2 V, Max. power current (I_{mpp}): 2.1 A, Open circuit voltage (V_{oc}): 52 V, Short circuit current (I_{sc}): 2.5 A, Irradiation: 1000 W/m².
3. Buck-Boost Converter: Input Voltage Range: 36V to 200V, Output Voltage: 71V, Voltage Ripple: 0.1V, Switching Frequency: 20 kHz, Load Current: 2.4 A, Duty Cycle (Min): 0.262, Duty Cycle (Max): 0.664, Inductor Value: 3.8 mH, Capacitor Value: 420 µF.

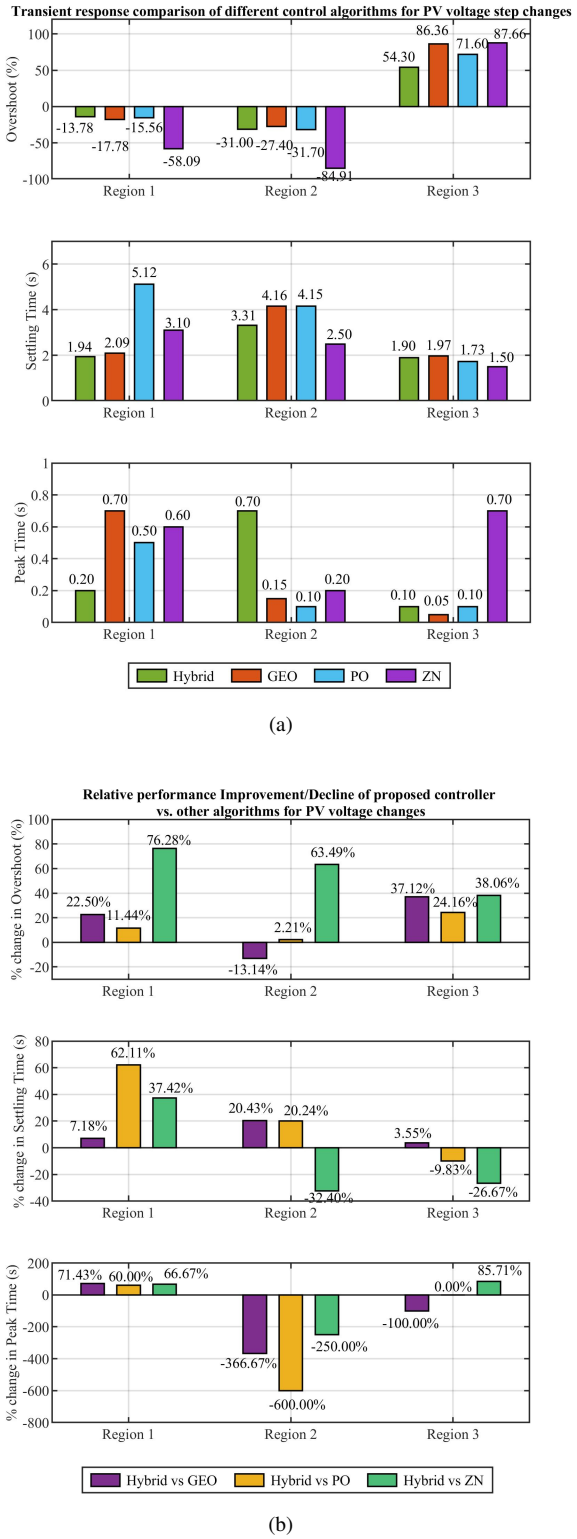

Fig. 15. (a) Transient Response Performance for PV step voltage changes: Proposed Hybrid GEO-PO algorithm vs. parent algorithms & ZN method. (b) Transient Response improvement of proposed GEO-PO algorithm vs. parent algorithms & ZN method for PV system voltage changes.

References

[1] M. S. Mastoi et al., "An in-depth analysis of electric vehicle charging station infrastructure, policy implications, and future trends," *Energy Reports*, vol. 8, pp. 11504–11529, Sep. 2022, doi: 10.1016/j.egyr.2022.09.011.

[2] K. A. Mamun et al., "Systematic Modeling and Analysis of On-Board Vehicle Integrated Novel Hybrid Renewable Energy System with Storage for Electric Vehicles," *Sustainability*, vol. 14, no. 5, p. 2538, Feb. 2022, doi: 10.3390/su14052538.

[3] S. M. Arif, T. T. Lie, B. C. Seet, S. Ayyadi, and K. Jensen, "Review of electric vehicle technologies, charging methods, standards and opti-

mization techniques," *Electronics*, vol. 10, no. 16, p. 1910, Aug. 2021, doi: 10.3390/electronics10161910.
[4] T. Imura, T. Yasuda, K. Oshima, T. Nayuki, M. Sato, and A. Oshima, "Wireless power transfer for electric vehicle at the kilohertz band," *IEEJ Transactions on Electrical and Electronic Engineering*, vol. 11, no. S2, Dec. 2016, doi: 10.1002/tee.22340.
[5] A. Sagar et al., "A comprehensive review of the recent development of wireless power transfer technologies for electric vehicle charging systems," *IEEE Access*, vol. 11, pp. 83703–83751, Jan. 2023, doi: 10.1109/access.2023.3300475.
[6] A. a. S. Mohamed, A. A. Shaier, H. Metwally, and S. I. Selem, "Wireless charging technologies for electric vehicles: Inductive, capacitive, and magnetic gear," *IET Power Electronics*, Dec. 2023, doi: 10.1049/pel2.12624.
[7] V. Ramya and R. Marimuthu, "A review on multi-input converters and their sources for fast charging of electric vehicles," *Engineering Science and Technology an International Journal*, vol. 57, p. 101802, Aug. 2024, doi: 10.1016/j.jestch.2024.101802.
[8] S. Athikkal, G. G. Kumar, K. Sundaramoorthy, and A. Sankar, "Performance analysis of novel bridge type dual input DC-DC converters," *IEEE Access*, vol. 5, pp. 15340–15353, Jan. 2017, doi: 10.1109/access.2017.2734328.
[9] S. Athikkal, G. G. Kumar, K. Sundaramoorthy, and A. Sankar, "A Non-Isolated Bridge-Type DC–DC converter for hybrid energy source integration," *IEEE Transactions on Industry Applications*, vol. 55, no. 4, pp. 4033–4043, May 2019, doi: 10.1109/tia.2019.2914624.
[10] S. Kumaravel, G. G. Kumar, K. Veeranna and V. Karthikeyan, "Novel Non-isolated Modified Interleaved DC-DC Converter to Integrate Ultracapacitor and Battery Sources for Electric Vehicle Application," *2018 20th National Power Systems Conference (NPSC), Tiruchirappalli, India, 2018*, pp. 1-6, doi: 10.1109/NPSC.2018.8771810.
[11] L. Kumar and S. Jain, "Multiple-input DC/DC converter topology for hybrid energy system," *IET Power Electronics*, vol. 6, no. 8, pp. 1483–1501, Aug. 2013, doi: 10.1049/iet-pel.2012.0309.
[12] M. Appikonda and D. Kaliaperumal, "Modelling and control of dual input boost converter with voltage multiplier cell," *IET Circuits Devices & Systems*, vol. 13, no. 8, pp. 1267–1276, Oct. 2019, doi: 10.1049/iet-cds.2019.0123.
[13] L. Colalongo, D. Dotti, A. Richelli, and Zs. M. Kovács-Vajna, "Non-isolated multiple-input boost converter for energy harvesting," *Electronics Letters*, vol. 53, no. 16, pp. 1132–1134, Jul. 2017, doi: 10.1049/el.2017.1590.
[14] G. G. Kumar, K. Sundaramoorthy, S. Athikkal, and V. Karthikeyan, "Dual input superboost DC–DC converter for solar powered electric vehicle," IET Power Electronics, vol. 12, no. 9, pp. 2276–2284, May 2019, doi: 10.1049/iet-pel.2018.5255.
[15] S. S. Dash and B. Nayak, "Control analysis and experimental verification of a practical dc–dc boost converter," *Journal of Electrical Systems and Information Technology*, vol. 2, no. 3, pp. 378–390, Dec. 2015, doi: 10.1016/j.jesit.2015.08.001.
[16] K. Kamalapathi, P. S. R. Nayak, and V. K. Tyagi, "Design and implementation of dual-source (WPT + PV) charger for EV battery charging," *International Transactions on Electrical Energy Systems*, vol. 31, no. 11, Sep. 2021, doi: 10.1002/2050-7038.13084.
[17] E. V. Paraskevadaki and S. A. Papathanassiou, "Evaluation of MPP voltage and power of MC-SI PV modules in partial shading conditions," *IEEE Transactions on Energy Conversion*, vol. 26, no. 3, pp. 923–932, Apr. 2011, doi: 10.1109/tec.2011.2126021.
[18] A. B, P. S. R. Nayak, S. K, and S. P. Simon, "'Systematic Analysis and Investigations on different Coil structures with misalignments for WPT System'.," *e-Prime - Advances in Electrical Engineering Electronics and Energy*, p. 100959, Mar. 2025, doi: 10.1016/j.prime.2025.100959.
[19] A. D. G. Jegha, M. S. P. Subathra, N. M. Kumar, U. Subramaniam, and S. Padmanaban, "A High Gain DC-DC Converter with Grey Wolf Optimizer Based MPPT Algorithm for PV Fed BLDC Motor Drive," *Applied Sciences*, vol. 10, no. 8, p. 2797, Apr. 2020, doi: 10.3390/app10082797.
[20] M. Appikonda and K. Dhanalakshmi, "Small-signal model and control approach for a dual input boost converter with VMC," *International Journal of Electronics*, vol. 109, no. 6, pp. 1035–1058, Aug. 2021, doi: 10.1080/00207217.2021.1966661.
[21] A. Mamizadeh, N. Genc and R. Rajabioun, "Optimal Tuning of PI Controller for Boost DC-DC Converters Based on Cuckoo Optimization Algorithm," *2018 7th International Conference on Renewable Energy Research and Applications (ICRERA)*, Paris, France, 2018, pp. 677-680, doi: 10.1109/ICRERA.2018.8566883.
[22] Rajasekaran, S., Suresh, S., Ramkumar, A. et al. A Novel Solar Photovoltaic Integrated Modified SEPIC High Gain DC–DC Converter Using Evolutionary Algorithms for Electric Vehicle Battery Applications. *J. Electr. Eng. Technol. 18*, 3681–3694 (2023). https://doi.org/10.1007/s42835-023-01459-2.
[23] Demir, Mehmet Hakan, and Mehmet Demirok. 2023. "Designs of Particle-Swarm-Optimization-Based Intelligent PID Controllers and DC/DC Buck Converters for PEM Fuel-Cell-Powered Four-Wheeled Automated Guided Vehicle" *Applied Sciences* 13, no. 5: 2919. https://doi.org/10.3390/app13052919.
[24] A. Ahmad et al., "Controller Parameters Optimization for Multi-Terminal DC power system using Ant Colony optimization," *IEEE Access*, vol. 9, pp. 59910–59919, Jan. 2021, doi: 10.1109/access.2021.3073491.
[25] A. Mohammadi-Balani, M. D. Nayeri, A. Azar, and M. Taghizadeh-Yazdi, "Golden eagle optimizer: A nature-inspired metaheuristic algorithm," *Computers & Industrial Engineering*, vol. 152, p. 107050, Dec. 2020, doi: 10.1016/j.cie.2020.107050.
[26] B. Abdollahzadeh et al., "Puma optimizer (PO): a novel metaheuristic optimization algorithm and its application in machine learning," *Cluster Computing*, vol. 27, no. 4, pp. 5235–5283, Jan. 2024, doi: 10.1007/s10586-023-04221-5.

M. Ganesh Babu received the B.Tech degree in Electrical and Electronics Engineering from Acharya Nagarjuna university AP, India in 2013. M. Tech degree from National Institute of Technology, Raipur, India in 2016. He is currently working towards the Ph.D. degree with National Institute of Technology, Trichy, India. His research interests include wireless charging in EV, Non-isolated dual-input converters optimization algorithms etc.

P. Srinivasa Rao Nayak received the B.Tech. degree in Electrical and Electronics Engineering from Nagarjuna University-Guntur AP, M. Tech. degree in Energy Systems from JNTUCE-JNTU Hyderabad, and the Ph.D. degree from the Department of Electrical Engineering, National Institute of Technology, Tiruchirappalli. Currently, he is an Associate Professor with the Department of Electrical and Electronics Engineering, National Institute of Technology, Tiruchirappalli, Tamil Nadu, India. His research interests include Power Electronic systems, Plug-in & Wireless EV Charging, Biologically Inspired Optimization Algorithm Techniques and Electric Vehicle Dynamics.